



OPEN ACCESS

EDITED BY
Mattias Collin,
Lund University,
Sweden

REVIEWED BY
Eric J. Sundberg,
Emory University,
United States
Bruce Turnbull,
University of Leeds,
United Kingdom

*CORRESPONDENCE
Kenneth K.-S. Ng
✉ Kenneth.Ng@uwindsor.ca
Jamshid Tanha
✉ Jamshid.Tanha@nrc-cnrc.gc.ca

[†]These authors have contributed equally to this work and share first authorship

SPECIALTY SECTION
This article was submitted to
Antimicrobials, Resistance and Chemotherapy,
a section of the journal
Frontiers in Microbiology

RECEIVED 28 November 2022
ACCEPTED 09 January 2023
PUBLISHED 26 January 2023

CITATION
Hussack G, Rossotti MA, van Faassen H,
Murase T, Eugenio L, Schrag JD, Ng KK-S and
Tanha J (2023) Structure-guided design of a
potent *Clostridioides difficile* toxin A inhibitor.
Front. Microbiol. 14:1110541.
doi: 10.3389/fmicb.2023.1110541

COPYRIGHT
© 2023 Hussack, Rossotti, van Faassen,
Murase, Eugenio, Schrag, Ng and Tanha. This is
an open-access article distributed under the
terms of the [Creative Commons Attribution
License \(CC BY\)](https://creativecommons.org/licenses/by/4.0/). The use, distribution or
reproduction in other forums is permitted,
provided the original author(s) and the
copyright owner(s) are credited and that the
original publication in this journal is cited, in
accordance with accepted academic practice.
No use, distribution or reproduction is
permitted which does not comply with these
terms.

Structure-guided design of a potent *Clostridioides difficile* toxin A inhibitor

Greg Hussack^{1†}, Martin A. Rossotti^{1†}, Henk van Faassen¹,
Tomohiko Murase², Luiz Eugenio², Joseph D. Schrag³,
Kenneth K.-S. Ng^{2,4*} and Jamshid Tanha^{1,5*}

¹Life Sciences Division, Human Health Therapeutics Research Centre, National Research Council Canada, Ottawa, ON, Canada, ²Department of Biological Sciences, University of Calgary, Calgary, AB, Canada, ³Life Sciences Division, Human Health Therapeutics Research Centre, National Research Council Canada, Montréal, QC, Canada, ⁴Department of Chemistry and Biochemistry, University of Windsor, Windsor, ON, Canada, ⁵Department of Biochemistry, Microbiology and Immunology, University of Ottawa, Ottawa, ON, Canada

Crystal structures of camelid heavy-chain antibody variable domains ($V_{\text{H}}\text{H}$ s) bound to fragments of the combined repetitive oligopeptides domain of *Clostridioides difficile* toxin A (TcdA) reveal that the C-terminus of $V_{\text{H}}\text{H}$ A20 was located 30Å away from the N-terminus of $V_{\text{H}}\text{H}$ A26. Based on this observation, we generated a biparatopic fusion protein with A20 at the N-terminus, followed by a (GS)₆ linker and A26 at the C-terminus. This A20-A26 fusion protein shows an improvement in binding affinity and a dramatic increase in TcdA neutralization potency (>330-fold [$I_{\text{C}_{50}}$]; $\geq 2,700$ -fold [$I_{\text{C}_{99}}$]) when compared to the unfused A20 and A26 $V_{\text{H}}\text{H}$ s. A20-A26 also shows much higher binding affinity and neutralization potency when compared to a series of control antibody constructs that include fusions of two A20 $V_{\text{H}}\text{H}$ s, fusions of two A26 $V_{\text{H}}\text{H}$ s, a biparatopic fusion with A26 at the N-terminus and A20 at the C-terminus (A26-A20), and actoxumab. In particular, A20-A26 displays a 310-fold ($I_{\text{C}_{50}}$) to 29,000-fold ($I_{\text{C}_{99}}$) higher neutralization potency than A26-A20. Size-exclusion chromatography-multiangle light scattering (SEC-MALS) analyses further reveal that A20-A26 binds to TcdA with 1:1 stoichiometry and simultaneous engagement of both A20 and A26 epitopes as expected based on the biparatopic design inspired by the crystal structures of TcdA bound to A20 and A26. In contrast, the control constructs show varied and heterogeneous binding modes. These results highlight the importance of molecular geometric constraints in generating highly potent antibody-based reagents capable of exploiting the simultaneous binding of more than one paratope to an antigen.

KEYWORDS

biparatopic, *Clostridioides difficile*, inhibitor, nanobody, single-domain antibody, toxin, $V_{\text{H}}\text{H}$

Introduction

Clostridioides difficile is a spore-forming Gram-positive bacterium capable of infecting humans and causing symptoms ranging from mild diarrhea to pseudomembranous colitis (Hussack and Tanha, 2016; Kordus et al., 2022). *C. difficile* infection is one of the most prevalent hospital-acquired bacterial infections, costing health-care systems ~\$5 billion per year and claiming up to 30,000 lives annually in the United States alone (Fu et al., 2021). The healthy balance of microbiota normally present in the gastrointestinal tract of individuals is thought to suppress *C. difficile* infection (Vasilescu et al., 2021). Changes to this balance, often *via* the introduction of broad-spectrum

antibiotics, can increase individuals' susceptibility to *C. difficile* colonization and infection. *C. difficile* remains an Urgent Threat pathogen according to the Centers for Disease Control and Prevention, despite numerous advances in new therapeutic agents to treat *C. difficile* infection.¹

C. difficile infection is currently treated with antibiotics that include metronidazole, vancomycin and fidaxomicin; however, significant incidences of disease relapse have made the search for alternative treatments, including vaccines (Henderson et al., 2017), fecal transplantation (Shogbesan et al., 2018) and antibody-based immunotherapy (Hussack and Tanha, 2016), a top public health priority. The primary virulence factors of *C. difficile* are two high molecular weight toxins (Kordus et al., 2022), toxin A (TcdA) and toxin B (TcdB), which are largely responsible for the physical damage in the colon of infected individuals and are the foremost targets of vaccine- and immunotherapy-based approaches (Hussack and Tanha, 2016; Henderson et al., 2017). Recently, a monoclonal antibody (mAb) targeting TcdB was shown to significantly reduce *C. difficile* relapse and was approved by the Food and Drug Administration. The trial data showed that reduced incidences of relapse were driven solely by the anti-TcdB mAb (bezlotoxumab) and not enhanced by the inclusion of an anti-TcdA mAb (actoxumab) in combination with bezlotoxumab (Wilcox et al., 2017). Interestingly, neither the TcdB antibody alone nor both mAbs in combination had a significant impact on the duration or severity of *C. difficile* infection (Wilcox et al., 2017), possibly due to the relatively poor efficacy of actoxumab. Several studies have illustrated that circulating anti-TcdA and TcdB antibodies in human patients correlate with reduced recurrence (Kyne et al., 2000, 2001; Leav et al., 2010), suggesting the development of TcdA inhibitors with considerably greater potency than actoxumab are warranted for use in combination with bezlotoxumab or other TcdB inhibitors. Efforts toward developing anti-toxin Ab-based therapeutics, including therapeutic approaches targeting both TcdA and TcdB, have been reviewed earlier (Hussack and Tanha, 2016).

Toward the goal of developing more effective therapeutics targeting TcdA, we previously isolated a panel of camelid single-domain antibodies (V_HHs or nanobodies) targeting *C. difficile* TcdA, including several V_HHs with the ability to neutralize TcdA cytotoxicity (Hussack et al., 2011). To better understand the determinants of molecular recognition and neutralization activity, we solved the crystal structures of two of these V_HHs targeting non-overlapping TcdA epitopes, namely A20.1 (A20) and A26.8 (A26), in complex with fragments from the combined repetitive oligopeptides (CROPs) domain of TcdA (Murase et al., 2014). These high-resolution crystal structures identified the specific locations of unique epitopes targeted by these antibodies and explained the synergistic TcdA neutralizing effects observed with these V_HHs (Hussack et al., 2011). While monomeric V_HHs and combinations of monomeric

V_HHs showed modest TcdA inhibition *in vitro*, we hypothesized that assembling the V_HHs as multimers and biparatopic dimers may improve TcdA neutralizing potency. Combining V_HHs in tandem, targeting distinct and/or common epitopes, has been successfully demonstrated for a number of anti-toxin V_HH systems, including: botulinum toxins (Mukherjee et al., 2012; Huang et al., 2017; Lam et al., 2020; Tremblay et al., 2020), anthrax toxin (Moayeri et al., 2015; Vrentas et al., 2016), ricin (Vance et al., 2013; Herrera et al., 2015, 2016), scorpion toxins (Hmila et al., 2008, 2010), Shiga toxins (Tremblay et al., 2013; Mejías et al., 2016), tetanus toxin (Rossotti et al., 2015), α -neurotoxin (Wade et al., 2022) and *C. difficile* TcdA and TcdB (Yang et al., 2014; Schmidt et al., 2016). In many of these examples, V_HH orientations were largely chosen at random, and the spacer lengths separating the two (or more) V_HH domains were typically not extensively explored.

The crystal structure of A20 and A26 bound to the C-terminal 255 residues of TcdA (amino acid residues 2,556–2,710 of TcdA10463; referred to as TcdA-A2 fragment; PDB 4NC1) revealed that the C-terminus of A20 was located 30 Å away from the N-terminus of A26 (Murase et al., 2014; Figure 1A). Molecular modeling led us to hypothesize that connecting A20 to A26 by a 12 residue (Gly-Ser)₆ linker would generate a biparatopic fusion protein in which the two tethered V_HH domains could simultaneously bind to a single molecule of TcdA, potentially generating a TcdA inhibitor with substantially higher binding affinity and inhibitory potency. To test this hypothesis, we have produced this biparatopic fusion protein and used *in vitro* binding and cytotoxicity inhibition measurements to confirm its high potency and specificity, capable of neutralizing TcdA at picomolar concentrations. The much weaker neutralization activities observed for a series of control constructs highlight the advantages of a structure-based approach in designing highly specific neutralization reagents and define some of the geometric constraints that are most critical for successfully combining V_HHs into biparatopic reagents. This study provides a dramatic example of how high-resolution crystal structures can be used to tailor the design of a multivalent toxin-inhibiting protein to match the molecular geometry of a toxin to generate novel and potent therapeutics.

Materials and methods

Structure-guided design of V_HH fusion proteins

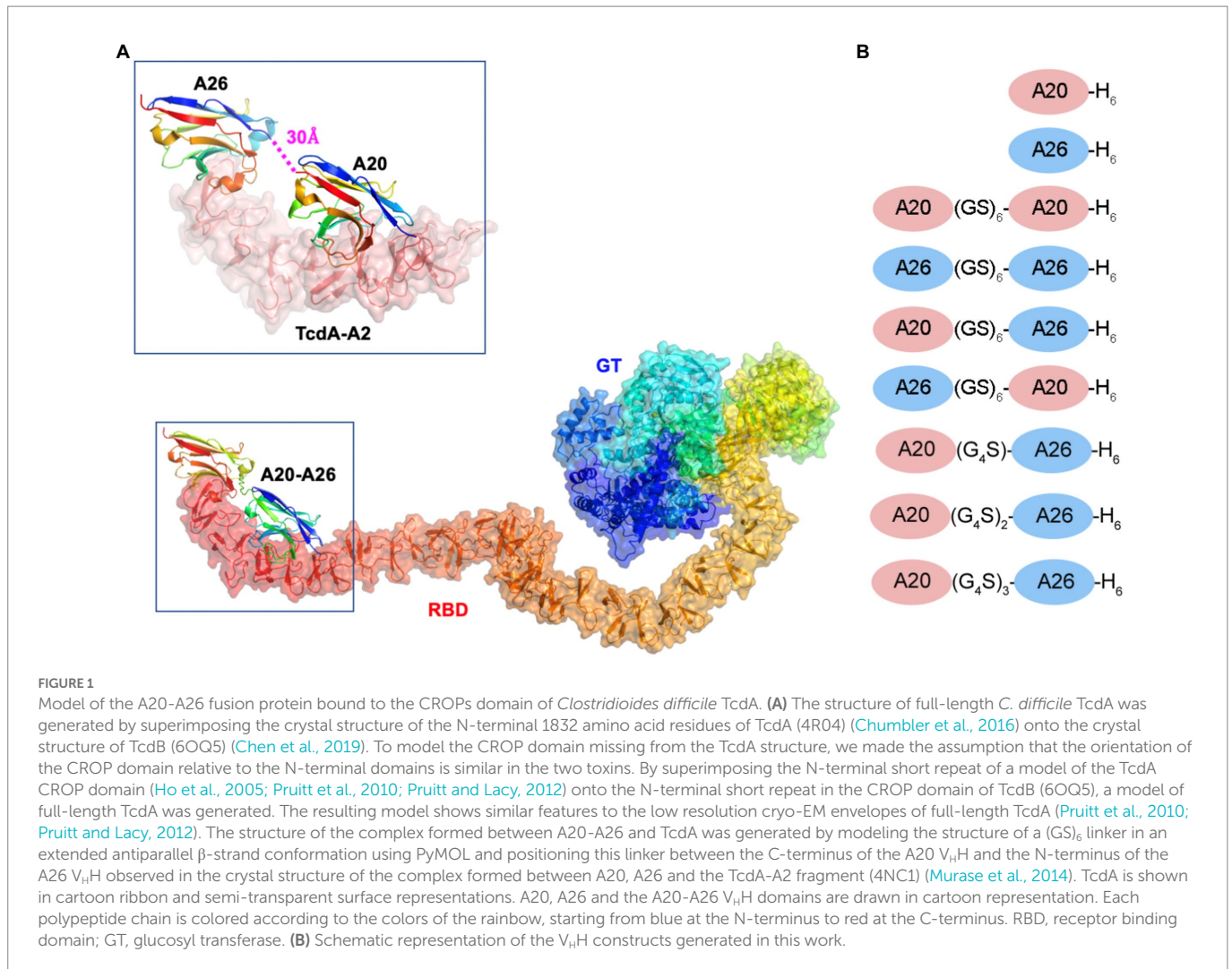
The ternary complex of the TcdA-A2 fragment bound to A20 and A26 (PDB 4NC1) indicated that the N-terminus of A26 was located 30 Å away from the C-terminus of A20. Models of linkers containing a repeating Gly-Ser dipeptide motif with backbone geometry similar to that seen in antiparallel β -strands were generated using PyMOL (Version 2.0, Schrödinger LLC). A linker with six (GS) dipeptides appeared to be sufficient to bridge the gap observed in the 4NC1 crystal structure, but the presence of disordered residues at the N- and C-termini of the V_HH proteins introduced a modest degree of uncertainty into the design. As a result, a series of constructs with a small range of linker lengths were generated.

Antibody expression and purification

V_HHs A20, A26, and B39 [anti-TcdB control V_HH; (Hussack et al., 2018)] were expressed in *Escherichia coli* TG1 cells as described

1 <https://www.cdc.gov/drugresistance/pdf/threats-report/clostridioides-difficile-508.pdf>

Abbreviations: CROP, combined repetitive oligopeptide domain of TcdA or TcdB; ELISA, enzyme-linked immunosorbent assay; PBS, phosphate-buffered saline; SEC-MALS, Size-exclusion chromatography-multiangle light scattering; SDS-PAGE, sodium dodecyl sulfate-polyacrylamide gel electrophoresis; SPR, surface plasmon resonance; TcdA, *Clostridioides difficile* toxin A; TcdB, *Clostridioides difficile* toxin B; V_HH, camelid heavy-chain antibody variable domain.



previously (Hussack et al., 2011). The optimized DNA sequences encoding A20-A20, A26-A26, A26-A20, A20-A26 (Hussack et al., 2011), and B39-B39 (Hussack et al., 2018) dimers were synthesized and subcloned into pTT5 (Durocher et al., 2002) expression plasmid (Thermo Fisher, Ottawa, Canada). The two monomer units in each dimer are separated by a (Gly-Ser)₆ linker sequence. Three additional A20-A26 constructs with Gly₄Ser, (Gly₄Ser)₂, and (Gly₄Ser)₃ amino acid linkers, hereafter referred to as A20-A26 (G₄S), A20-A26 (G₄S)₂, and A20-A26 (G₄S)₃, were also subcloned into pTT5. All V_HH dimers, the anti-TcdA IgG1 reference antibody actoxumab (CDA1) and the anti-TcdB IgG1 reference antibody bezlotoxumab (MDX1388) were expressed in HEK293-6E cells as described (Hussack et al., 2018). Five days after the transfection, supernatants were harvested by centrifugation at 3,000 × g for 10 min and filtered through 0.2- μ m filter (Millipore, Etobicoke, Canada), dialyzed against phosphate-buffered saline (PBS) overnight at 4°C, and then the His₆-tagged dimers were purified by immobilized metal-ion affinity chromatography using a HisTrap column (Cytiva Life Sciences, Mississauga, Canada) and an AKTÄ™ FPLC (Cytiva Life Sciences). CDA1 and MDX1388 were purified by protein A affinity chromatography. The eluted proteins were buffer exchanged into PBS using Amicon devices, sterilized through 0.2- μ m filtration and stored at -80°C. Antibody concentrations were determined from their respective molar extinction coefficients and A₂₈₀

absorbance, measured on a NanoDrop 3300 fluorospectrometer (Thermo Fisher). Protein purity was assessed by reducing and non-reducing sodium dodecyl sulfate-polyacrylamide gel electrophoresis (SDS-PAGE).

Size-exclusion chromatography

Purified proteins (400 μ g in PBS) were loaded onto a Superdex™ 75 Increase 10/30 GL (Cytiva Life Sciences) column, at a flow rate of 0.5 mL/min, controlled by an AKTÄ™ FPLC (Cytiva Life Sciences). To determine the size of each construct, a standard curve was generated using the Bio-Rad™ Size-Exclusion Chromatography Standard (BioRad, Hercules, CA) and apparent molecular masses (M_{app}) of antibodies were calculated by interpolation using their elution volumes (V_e s). Size-exclusion chromatography (SEC) chromatograms were normalized as described (Kim et al., 2012).

Enzyme-linked immunosorbent assay

Nunc-immuno microtitre plate wells with Maxisorp surface (Thermo Fisher) were coated in triplicates with 30 ng/well of full-length

TcdA (List Biological Laboratories, Inc., Campbell, CA) in 0.05 M carbonate–bicarbonate buffer pH 9.6, and incubated overnight at 4°C. Wells were blocked with 1% (w/v) bovine serum albumin in PBS for 1 h at room temperature, washed with PBS/0.05% (v/v) Tween 20 and then incubated for 1 h with decreasing concentrations of His₆-tagged V_HH constructs in PBS containing 0.2% bovine serum albumin and 0.05% Tween 20 (PBS-TB). Following washing, the binding to TcdA was probed by incubating the wells for 1 h at room temperature with 0.2 ng/mL polyclonal rabbit anti-His₆ antibody conjugated to horseradish peroxidase (Bethyl Laboratories, Montgomery, TX) in PBS-TB. Wells were washed and incubated at room temperature for 15 min with 100 μL TMB peroxidase substrate solution (KPL, Gaithersburg, MD). Then, 50 μL of 1 M H₂SO₄ was added to stop enzymatic reactions and absorbance was read at 450 nm on a Multiskan Enzyme-linked immunosorbent assay (ELISA) plate reader (Thermo Fisher). Data analysis was performed using Prism software version 8.3 (GraphPad Software, Inc., La Jolla, CA).

Surface plasmon resonance analysis

All surface plasmon resonance (SPR) experiments were performed on a Biacore 3000 instrument (Cytiva Life Sciences) at 37°C in HBS-EP running buffer (10 mM HEPES, pH 7.4, 150 mM NaCl, 3 mM EDTA, 0.005% (v/v) surfactant P20). Recombinant TcdA-A2 fragment (Greco et al., 2006), encompassing the C-terminal CROPs domain of TcdA (aa 2,556–2,710) from *C. difficile* reference strain 10463, was amine coupled to a CM5 sensor chip at pH 4.5 in acetate buffer using standard methods recommended by the manufacturer (Cytiva Life Sciences) to create a high-density toxin A surface with ~8,500 resonance units immobilized. An ethanolamine-blocked flow cell served as a reference surface. The flow rate for all experiments was 40 μL/min and SEC-purified antibodies were injected for 120 s at a single concentration that varied depending on the antibody (CDA1: 50 nM; A26 and B39: 10 nM; A20: 5 nM; A20-A20, A26-A26, A20-A26 and A26-A20: 1 nM). Antibody dissociation was followed for 300 s for the monomeric antibodies (A20, A26, and B39) and 3,600 s for the bivalent antibodies (A20-A20, A26-A26, A20-A26, A26-A20 and CDA1). Complete regeneration of the TcdA-A2 surface was achieved with a 6 s pulse of 10 mM glycine, pH 2.0, for all antibodies except CDA1 (12 s pulse of 5 mM NaOH), all at a flow rate of 100 μL/min. Off-rates ($k_{d,s}$, s⁻¹) were determined by fitting the dissociation phase (1,500–3,500 s for bivalent antibodies, 150–300 s for A20, 130–200 s for A26) of each sensorgram to a separate k_d 1:1 binding model using the BIAevaluation v4.1 software (Cytiva Life Sciences). With one exception (A20-A26), all antibodies achieved the minimum 5% dissociation required to accurately report an off-rate (Katsamba et al., 2006).

In vitro TcdA neutralization assay

Vero cells (CCL-81) were obtained from ATCC (Manassas, VA) and cultured according to ATCC's instructions in 96 well microtiter plates (Nunc) at 2 × 10⁴ cells/well in MEM media (Gibco) supplemented with 10% (v/v) heat-inactivated fetal bovine serum (Gibco) at 37°C in 5% CO₂. The neutralization activity of antibodies was determined by co-incubation with 80 ng/mL (260 pM) of full-length TcdA, with antibody and toxin added simultaneously to the cells. After 72 h of incubation, the cell viability was quantified with the Cell Proliferation

Assay Reagent WST-1 (Roche Diagnostics, Laval, Canada) according to the manufacturer's instructions. Briefly, the media was replaced with 100 μL of MEM (without fetal bovine serum) containing 10% of WST-1, incubated for 40 min at 37°C in 5% CO₂ and finally the absorbance read at 450 nm. The neutralizing activity was calculated as % inhibition:

$$\% \text{ Inhibition} = \frac{A450_{\text{test}} - A450_{\text{low}}}{A450_{\text{high}} - A450_{\text{low}}} \times 100$$

A450_{test} is the absorbance of cells incubated with TcdA and varying concentrations of antibodies;

A450_{low} is the absorbance of cells incubated only with TcdA (0% inhibition); and

A450_{high} is the absorbance of cells incubated only with media (100% inhibition).

UPLC-SEC-multiangle light scattering analysis

Monomeric and dimeric V_HHs were mixed with TcdA-A2 at 1:1 molar ratios in PBS at final concentrations of 1.91 mg/mL and incubated at 4°C overnight. Control experiments which included monomeric V_HHs alone (0.91 mg/mL), dimeric V_HHs alone (0.91 mg/mL) and TcdA-A2 alone (1 mg/mL) were performed under the same conditions as the V_HH-TcdA-A2 mixtures. UPLC-SEC analysis of protein samples was performed on a BEH200 SEC column (4.6 × 150 mm, 1.7 μm particle column, Waters, Milford, MA) using a Waters H-Class Acquity UPLC system equipped with a diode array detector, a Wyatt MiniDawn multiangle light scattering (MALS) detector, and a Wyatt Optilab T-rEX refractive index detector (Wyatt Technology, Santa Barbara, CA). The mobile phase was PBS (HyClone SH30028.02, Cytiva Life Sciences) containing 0.02% (v/v) polysorbate 20 at a flow rate of 0.4 mL/min. The column temperature was 30°C. Molar masses were determined using Astra software version 6.1.7.17 (Wyatt Technology) using either absorbance at 280 nm (A₂₈₀) or refractive index (RI) as the concentration measure. Similar results were obtained using either A₂₈₀ or RI, but band broadening reduced resolution in the RI signal so masses determined using the A₂₈₀ signal are reported.

Results

Structure-guided design of V_HH fusion proteins

We previously solved the X-ray structures of two *C. difficile* TcdA-binding V_HHs, A20 (K_D = 2 nM) and A26 (K_D = 12 nM), in complex with fragments from the CROPs domain (formerly referred to as the RBD, receptor binding domain) of TcdA (Hussack et al., 2011; Murase et al., 2014). Because in the ternary complex of the TcdA-A2 fragment bound to a single molecule of A20 and a single molecule of A26 (PDB 4NC1) the N-terminus of A26 was observed to be located 30 Å away from the C-terminus of A20, we hypothesized that a short linker peptide could be used to fuse the two V_HH domains together in a recombinant fusion protein (Figure 1). Models of linkers containing a repeating Gly-Ser dipeptide motif were generated with backbone geometry similar to that seen in antiparallel β-strands. A linker with six Gly-Ser dipeptides (GS)₆

appeared to be sufficient to bridge the gap observed in the 4NC1 crystal structure, but the presence of disordered residues at the N- and C-termini of the V_HH proteins indicate that the ideal lengths and geometric details of linkers is challenging to model precisely. As a result, in addition to A20-A26 with a (GS)₆ linker, a series of constructs with a range of linker lengths were generated (Figure 1B). These included A20-A26 (G₄S), A20-A26 (G₄S)₂, and A20-A26 (G₄S)₃, which possessed linkers of shorter [(G₄S)], similar [(G₄S)₂] and longer [(G₄S)₃] distances than the (GS)₆ construct. The crystal structures also clearly indicated that the polarity of the arrangement of V_HH domains (i.e., whether the A20 V_HH domain or the A26 V_HH domain is N-terminal to the other V_HH domain in the fusion protein) would likely be critical, as the reverse orientation of V_HH domains would not be expected to allow for the simultaneous binding of both V_HH domains to the same molecule of TcdA. To test this prediction, the A26-A20 fusion protein was generated with the reverse polarity (i.e., A26 at the N-terminus and A20 at the C-terminus). To evaluate whether the tethering of two V_HH domains generates a non-specific multivalency effect, two other fusion proteins containing two A20 V_HH domains (A20-A20) and two A26 V_HH domains (A26-A26), each tethered by the (GS)₆ linker, were also generated.

Expression, purification and biophysical characterization of V_HH fusion proteins

While monomeric V_HHs were expressed in the periplasm of *E. coli*, the dimeric V_HHs were expressed in mammalian HEK293-6E cells to obtain higher expression yields. Nonetheless, in contrast to A20-A26 (G₄S) and A20-A26 (G₄S)₂, which could be expressed in high yields similar to the dimers with the (GS)₆ linker (Table 1), the A20-A26 (G₄S)₃ construct was surprisingly only expressed at very low yields despite repeated attempts, excluding its full analysis in the current study. The proteins were purified by immobilized metal-ion affinity chromatography and ran as single bands of the expected molecular masses on SDS-PAGE under reducing and non-reducing conditions (Figure 2A). Control proteins (V_HH B39, V_HH-V_HH B39-B39, mAbs CDA1 and MDX1388) were expressed in *E. coli* or HEK293-6E cells and purified by immobilized metal-ion affinity chromatography or protein A affinity chromatography (data not shown). Purified yields of A20 and A26 were in the range of 15–20 mg/L, and yields of the four dimeric V_HHs ranged from 80–114 mg/L (Table 1). The SEC profiles of all V_HHs

and V_HH dimers produced single, monodispersed peaks devoid of aggregates (100% “monomeric”) with V_s consistent for a V_HH monomer to dimer transition and relative to protein standards (Figure 2B; Table 1).

Binding of V_HHs and V_HH-V_HHs to immobilized TcdA was demonstrated by ELISA (Figure 2C; Table 1). The four dimeric constructs, A20-A20, A26-A26, A20-A26 and A26-A20, showed the strongest binding to TcdA with similar apparent EC₅₀s of 32–47 pM. In contrast, monomeric A20 and A26 demonstrated significantly lower TcdA binding, with EC₅₀s of 194 pM (A20) and 14.6 nM (A26). The off-rates (k_d, s⁻¹) of all constructs were determined by SPR by flowing V_HHs, V_HH-V_HHs or control CDA1 mAb over amine coupled TcdA for long dissociation times at 37°C (Figure 2D; Table 1). Consistent with the ELISA results, A20 and A26 dissociated rapidly with k_ds of 2.5 × 10⁻² s⁻¹ and 7.5 × 10⁻³ s⁻¹, respectively. All dimeric constructs clearly showed avid binding and demonstrated very slow dissociation rates as expected; however, subtle differences were evident. Of the dimeric proteins, A26-A26 dissociated the fastest followed by A20-A20 and A26-A20, which had similar k_ds to the CDA1 IgG benchmark. The dissociation of A20-A26 was very slow (6.9 × 10⁻⁶ s⁻¹), which is at the instrument limit of detection, achieving only 4% dissociation after an hour and corresponding to an estimated half-life of 28.1 h (Table 1).

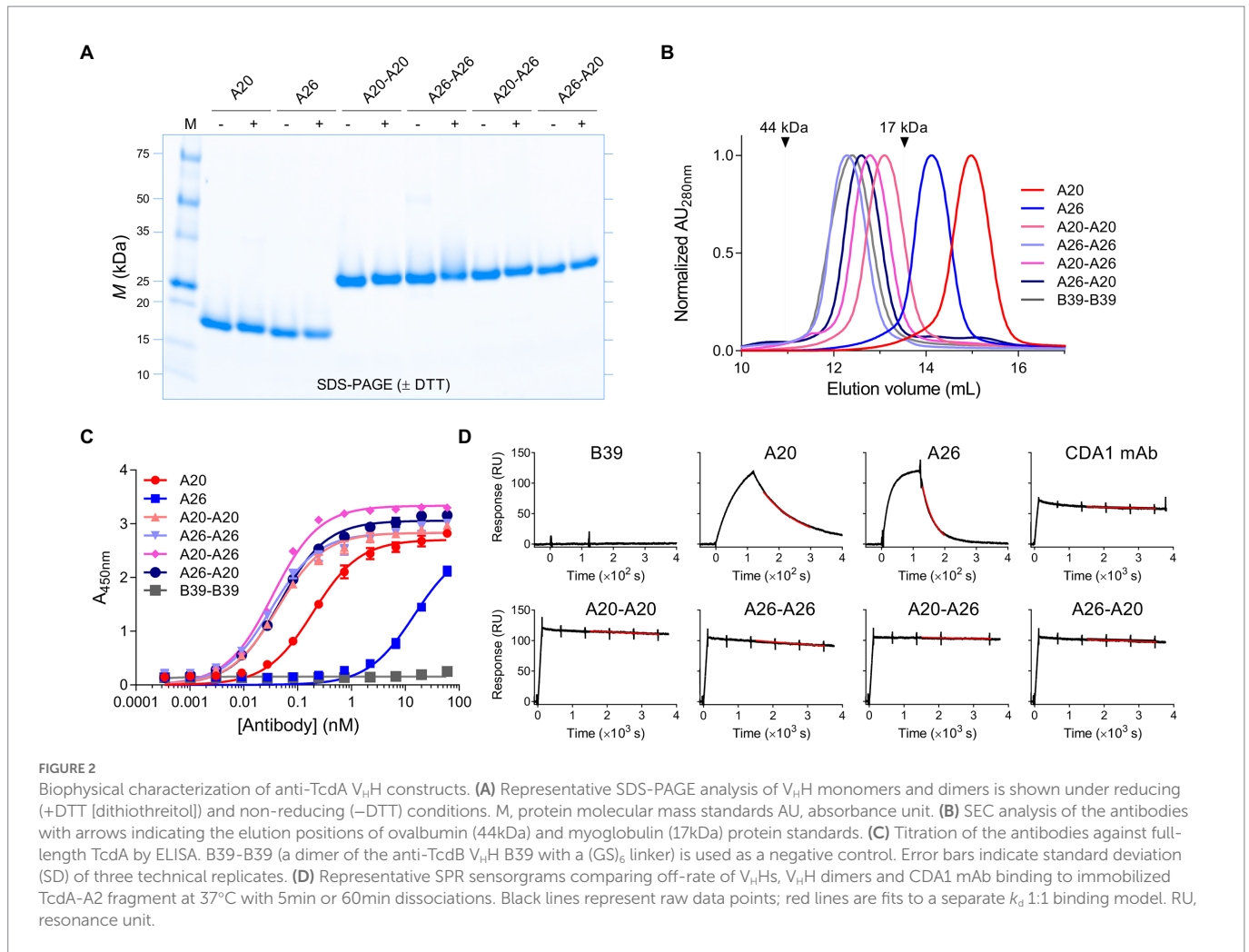
In vitro TcdA neutralization

We compared the TcdA neutralizing potency of the various V_HH constructs and controls in a 72 h TcdA inhibition assay using Vero cells. Initially, toxin neutralization was performed on monomers, dimers and the CDA1 benchmark mAb at a concentration of 100 nM (Figure 3A). The A20-A26 construct was a superior neutralizer in comparison to other monomers (A20, A26, and A20 + A26), dimers (A20-A20, A26-A26, and A26-A20) and CDA1, reaching nearly 100% TcdA neutralization. Moreover, while A26 demonstrated significant TcdA inhibition, A20 did not show any despite its higher affinity for TcdA, underlining the critical role epitope location plays in TcdA neutralization. Next, we performed neutralization experiments with various antibody concentrations (Figure 3B) to determine IC₅₀, IC₉₉ and maximum toxin inhibition values (Table 2). Antibody titration curves demonstrated a dramatic shift in neutralizing potency of A20-A26 relative to the other mono- and biparatopic constructs tested. The IC₅₀ of A20-A26 (0.16 nM) was far superior to A26-A20 (49.7 nM), A20-A20 (174.5 nM), A26-A26 (39 nM), and CDA1 (30 nM). The IC₉₉ of A20-A26 (0.27 nM) was even more dramatic in relation to comparators A26-A20

TABLE 1 Biophysical properties of anti-TcdA V_HH constructs.

Antibody	Linker	M _r (Da)	Yield (mg/L)	Mon. (%) ^c	EC ₅₀ (pM) ^d	k _d (s ⁻¹) ^e	Dissociation (%) ^f	T _{1/2} (h) ^g
A20	na	15,670	19 ^a	100	194 ± 13	(7.5 ± 0.1) × 10 ⁻³	88.4 ± 0.3	0.03
A26	na	16,016	15 ^a	100	14,620 ± 2,320	(2.5 ± 0.1) × 10 ⁻²	98.9 ± 0.2	0.01
A20-A20	[GS] ₆	28,679	80 ^b	100	42 ± 3	(1.8 ± 0.2) × 10 ⁻⁵	7.7 ± 1.1	10.6
A26-A26	[GS] ₆	29,371	110 ^b	100	32 ± 3	(3.6 ± 0.4) × 10 ⁻⁵	13.5 ± 0.7	5.4
A20-A26	[GS] ₆	29,025	114 ^b	100	34 ± 2	(6.9 ± 1.5) × 10 ⁻⁶	3.9 ± 0.5	28.1
A26-A20	[GS] ₆	29,025	112 ^b	100	47 ± 2	(1.7 ± 0.2) × 10 ⁻⁵	7.5 ± 1.1	11.3
CDA1 IgG	na	145,580	80	nd	nd	(2.2 ± 0.2) × 10 ⁻⁵	18.0 ± 0.6	8.8

na, not applicable; nd, not determined. ^aProtein purification yield from 1 L *E. coli* cultures. ^bProtein purification yield extrapolated from 100 mL HEK293-6E cultures. ^cPercent monomer peak area determined from size exclusion chromatograms. ^dDetermined by ELISA. ^eDetermined by SPR at 37°C with a 5 min (monomers) or 60 min (dimers, mAb) dissociation. Values are mean ± SD from three technical replicates. ^fPercent dissociation of SPR response after 5 min (monomers) or 60 min (dimers, mAb). Values are mean ± SD from three technical replicates. ^gSPR-calculated half-life (T_{1/2} = 0.693/k_d).



(7,866 nM), A20-A20 (2,123 nM), A26-A26 (1,189 nM) and CDA1 (3,342 nM). In particular, relative to the reverse orientation control A26-A20 and CDA1, A20-A26 outperformed these antibodies by 29,000- and 12,500-fold, respectively. Antibody efficacy, reported as the maximum level of TcdA inhibition achieved, was also superior for the A20-A26 construct reaching 94% compared to A26-A20 (85%), A20-A20 (85%), A26-A26 (89%) and CDA1 (78%).

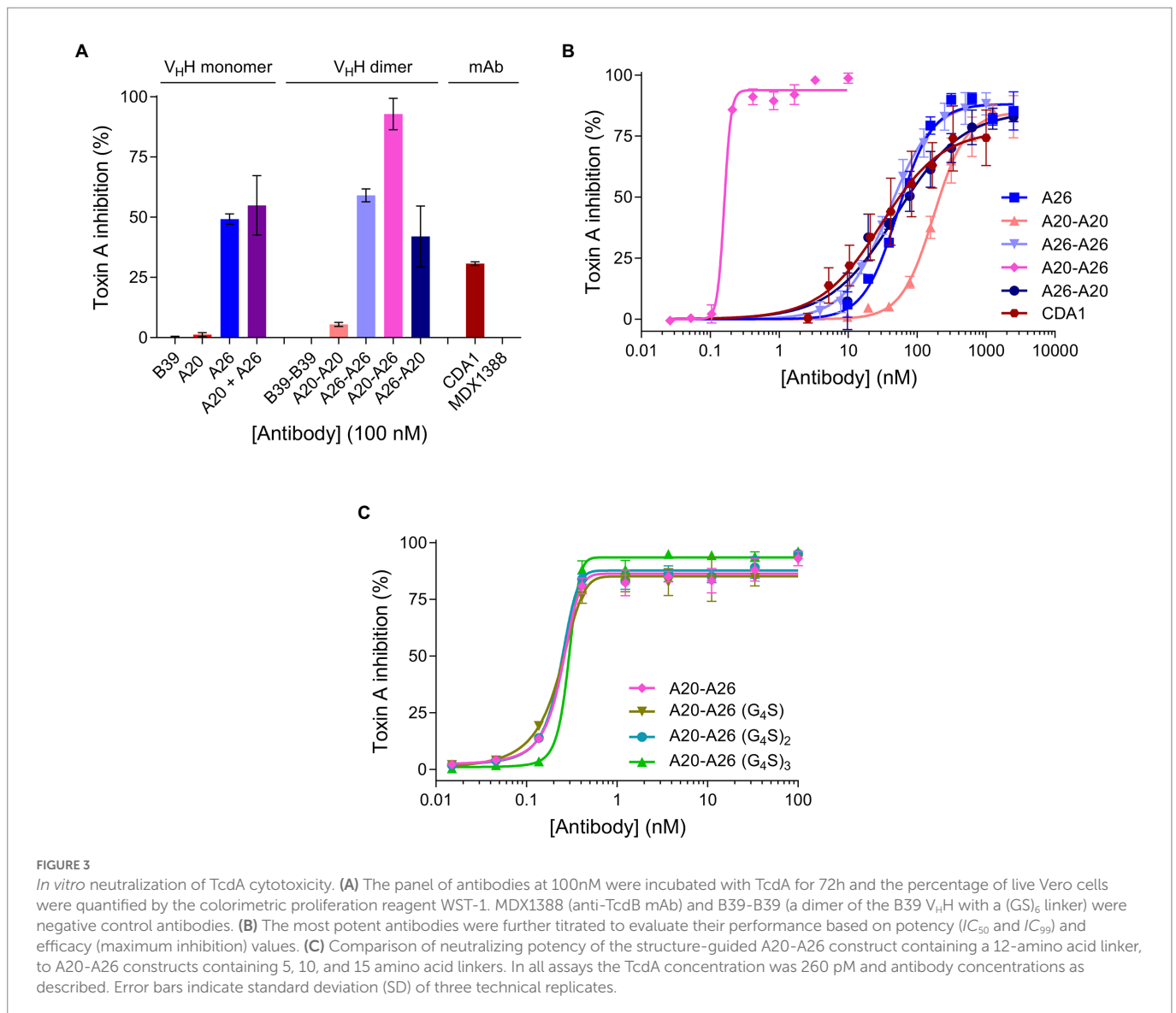
Given the potency of A20-A26, three additional constructs were designed with varying linker lengths of (G_4S) , $(G_4S)_2$, and $(G_4S)_3$ separating the two V_H Hs. Neutralization experiments comparing the original A20-A26 construct containing the $(GS)_6$ linker with the various G_4S linkers revealed essentially identical neutralizing potency (Figure 3C). This is reflected in similar IC_{50} (0.16 nM, 0.22 nM, 0.23 nM, and 0.29 nM) and IC_{99} (0.27 nM, 0.54 nM, 0.42 nM, and 0.46 nM) values for A20-A26, A20-A26 (G_4S), A20-A26 (G_4S)₂, and A20-A26 (G_4S)₃, respectively (Table 2). The antibody efficacy of A20-A26 (94%) slightly exceeded constructs with shorter linkers A20-A26 (G_4S) (85%) and A20-A26 (G_4S)₂ (88%), and was essentially the same as the construct with a longer linker A20-A26 (G_4S)₃ (94%) (Table 2).

UPLC-SEC-MALS analysis of V_H H-TcdA complexes

To gain further insight into the mechanism of action underlying the high neutralization potencies observed with A20-A26 dimers, several

monomeric and dimeric V_H Hs were incubated with TcdA-A2 in solution at 1:1 molar ratios for formation of antibody-TcdA-A2 complexes. The toxin/antibody mixtures were then subjected to SEC-MALS analysis to obtain observed molecular masses (M_{obs}) and retention times (T_r s) of free (TcdA-A2 [Ag], antibody [Ab]), and complexed (Ag.Ab) species. M_{obs} and T_r values, complemented with neutralization data, were used to determine the types of binding complexes ("species" and "modes") formed (Figure 4; Table 3).

As expected, the individual unmixed TcdA-A2 and V_H H samples treated under the same conditions as the Ag-Ab mixes had M_{obs} very close to the theoretical M_r values, indicating the lack of significant homotypic interactions for each individual protein. The M_{obs} for A20:TcdA-A2 and A26:TcdA-A2 complexes were consistent with a 1:1 TcdA-A2- V_H H complex type (Ag.Ab) and the previous SEC data obtained for these complexes (Murase et al., 2014). The extent of complex formation was higher for A20 (80%) than for A26 (69%), consistent with its higher affinity for TcdA-A2 (Hussack et al., 2011). Homodimeric A20-A20 gave a major complex (92%) of (Ag)₂.Ab type and a minor complex (8%) of Ag.Ab type. For the A26-A26 homodimer, however, it was not clear from the M_{obs} , whether the complex was of Ag.Ab or (Ag)₂.Ab type for the major SEC species (76%) or of Ag.Ab or Ag type for the minor SEC species (24%) due to intermediary M_{obs} values relative to expected M_r s. Nonetheless, all possible complexes point to a lack of binding avidity. Thus, as in the case of A20 vs A26 V_H H, a higher % of complex formation for A20-A20 may be due to a higher intrinsic affinity of A20 for TcdA-A2. Moreover, the lack of binding



avidity explains why A26 and A26-A26 have similar potencies, and in the case of A20-A20, it suggests the acquired neutralization capability of A20 upon homodimerization may be due to increased steric hindrance.

A20-A26 formed predominantly an Ag.Ab type complex (91%), and along with its ultra-potent neutralization capability, indicates that both V_HH domains in A20-A26 simultaneously engage with a single molecule of TcdA-A2 in a biparatopic fashion with 1:1 stoichiometry (Mode 1), as predicted from the original design based on the crystal structure (Figure 4). Conversely, A26-A20 did not appear to form any biparatopic complexes, a result that is also consistent with the crystal structure predictions. It formed two major complexes at 55% and 43% with significantly different *T_r*s but similar *M_{obs}*s, indicative of (Ab)₂(Ag)₂ tetrameric (Modes 2, 3, and 4) and (Ab)₂Ag and/or Ab.(Ag)₂ trimeric complexes (Modes 5 and 6), respectively. Of the three tetrameric possibilities, one can adopt a cross-biparatopic binding arrangement (Mode 2), while the other two arrange in such a manner that excludes binding avidity (Modes 3 and 4, Figure 4). The far weaker neutralization potency of the A26-A20 construct relative to the A20-A26 biparatopic construct, on the one hand, and its similar neutralization capability to

monomeric and homodimeric A20/A26 constructs, on the other, indicate that only one V_HH domain in A26-A20 is able to bind to a single epitope in TcdA-A2 within any one particular molecular complex, thus excluding the possibility of Mode 2 binding. Interestingly, A20-A26 (G₄S) and A20-A26 (G₄S)₂ which had the same V_HH-V_HH orientations as A20-A26, formed complexes with *M_{obs}*s consistent with Mode 1 and Mode 2 biparatopic Ab.Ag engagement. Molecular models based on the crystal structures indicate that the much shorter linker found in A20-A26 (G₄S) when compared with A20-A26 would likely prevent the formation of complexes where both of the A20 and A26 V_HH domains are able to bind to a single molecule of TcdA-A2 simultaneously. This likely explains why only 53% of the complexes detected for A20-A26 (G₄S) show 1:1 stoichiometry (Ab.Ag; Mode 1), whereas 47% of the complexes show 2:2 stoichiometry ((Ab)₂(Ag)₂; Mode 2) based on the *M_{obs}* and *T_r* parameters. In comparison, 91% of the complexes formed by A20-A26 and A20-A26 (G₄S)₂, which both have linkers with similar lengths that are expected to allow both V_HH domains to bind simultaneously to a single molecule of TcdA-A2, show 1:1 stoichiometry (Ab.Ag; Mode 1). Only up to 9% of the complexes have 2:2 stoichiometry ((Ab)₂(Ag)₂; Mode 2). A20-A26 (G₄S)₃ was not analyzed by SEC-MALS,

TABLE 2 TcdA neutralizing potency and efficacy of V_HH constructs.

Antibody	Linker	TcdA inhibition		
		IC ₅₀ (nM)	IC ₉₉ (nM) ^a	Efficacy (%) ^b
A20	na	–	–	–
A26	na	52.6 ± 3.2	719	88.1 ± 1.7
A20-A20	[GS] ₆	174.5 ± 12.5	2,123	84.9 ± 2.4
A26-A26	[GS] ₆	39.0 ± 2.9	1,189	89.1 ± 2.1
A20-A26	[GS] ₆	0.16 ± 0.01	0.27	93.8 ± 1.0
A26-A20	[GS] ₆	49.7 ± 9.1	7,866	85.3 ± 4.2
CDA1 IgG	na	30.0 ± 8.1	3,342	77.5 ± 6.2
A20-A26 (G ₄ S)	[G ₄ S]	0.22 ± 0.02	0.54	85.1 ± 1.2
A20-A26 (G ₄ S) ₂	[G ₄ S] ₂	0.23 ± 0.02	0.42	87.7 ± 1.1
A20-A26 (G ₄ S) ₃	[G ₄ S] ₃	0.29 ± 0.02	0.46	93.5 ± 0.8

Vero cell cytotoxicity assays measuring mean ± SD TcdA inhibition after 72 h, from three technical replicates, shown in Figures 3B,C. na, not applicable; –, lack of neutralization activity (at 100 nM V_HH concentration). ^aCalculated from mean IC₅₀ value and Hill slope. ^bMaximum level of TcdA inhibition.

because it could not be expressed in sufficient quantities. However, it is expected to possess a similar binding mode to that observed for A20-A26 and A20-A26 (G₄S)₂, because the longer linker length would be expected to allow both V_HH domains to bind to a single molecule of TcdA-A2 simultaneously.

Discussion

In this work we used the crystal structures of V_HHs A20 and A26 in complex with *C. difficile* TcdA that we had previously determined to guide the design of a novel and ultra-potent toxin inhibitor which we have named A20-A26. This fusion protein is comprised of the A20 V_HH at the N-terminus, followed by a 12 residue (GS)₆ linker and then the A26 V_HH at the C-terminus. A20-A26 expressed well in mammalian cells (>100 mg/L), and was monodispersed and free of aggregates. A20-A26 also showed high, avidity-driven apparent binding affinities for immobilized TcdA and TcdA in solution. Most importantly, A20-A26 was extremely potent at neutralizing TcdA in cytotoxicity assays with Vero cells, achieving a ≥2,700-fold improvement in potency

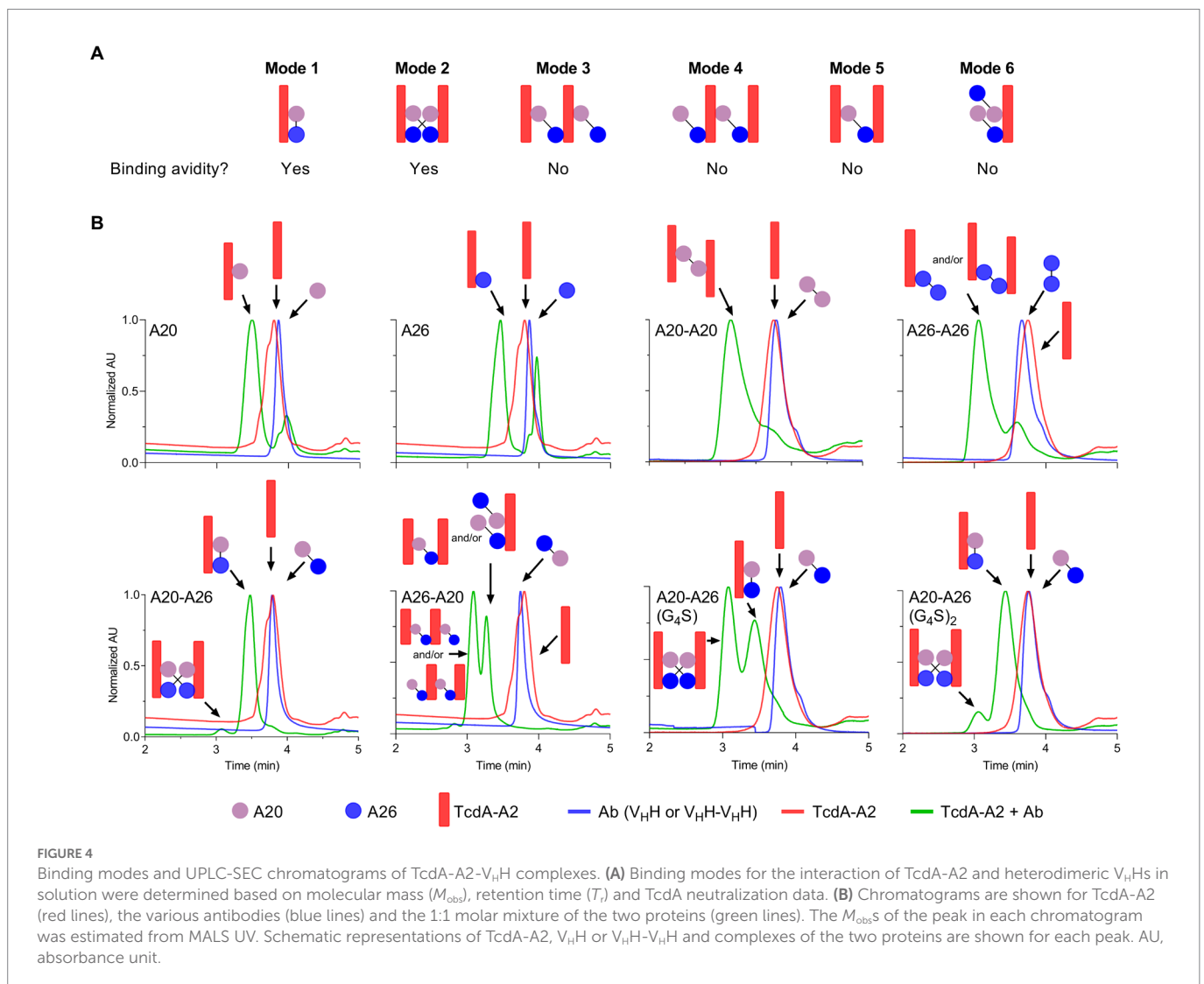


TABLE 3 SEC-MALS derived molecular masses for TcdA-A2+V_HH complexes.

Sample	T_r (min)	M_r (kDa)	M_{obs} (kDa)	Species	Relative proportion (%) ^{a,b}
TcdA-A2	3.748 ± 0.001	32.1	31.3 ± 1.1	Ag	100
A20	3.864 ± 0.001	16.3	17.9 ± 0.1	Ab	100
A26	3.866 ± 0	16.0	18.5 ± 2.1	Ab	100
A20-A20	3.786 ± 0.001	28.7	28.6 ± 2.6	Ab	100
A26-A26	3.665 ± 0.001	29.4	25.4 ± 0.6	Ab	100
A20-A26	3.786 ± 0.001	29.0	29.6 ± 0.6	Ab	100
A26-A20	3.745 ± 0.001	29.0	29.2 ± 0.2	Ab	100
A20-A26 (G ₄ S)	3.792 ± 0.001	28.5	26.1 ± 0.5	Ab	100
A20-A26 (G ₄ S) ₂	3.767 ± 0.002	28.8	24.1 ± 1.0	Ab	100
TcdA-A2 + A20	3.493 ± 0.001	48.4 [Ag,Ab]	41.1 ± 0	Ag,Ab	79.6
	3.974 ± 0.001	16.3 [Ab]	19.5 ± 0.5	Ab	16.3
	–	–	–	–	4.1
TcdA-A2 + A26	3.470 ± 0	48.1 [Ag,Ab]	41.1 ± 0.2	Ag,Ab	69.2
	3.969 ± 0	16.0 [Ab]	16.4 ± 0.7	Ab	27.0
	–	–	–	–	3.7
TcdA-A2 + A20-A20	3.145 ± 0.004	92.9 [(Ag) ₂ ,Ab]	77.3 ± 0.9	(Ag) ₂ ,Ab	92.4
	3.754 ± 0.002	60.8 [Ag,Ab]	65.1 ± 5.9	Ag,Ab	7.5
TcdA-A2 + A26-A26	3.060 ± 0.001	93.6 [(Ag) ₂ ,Ab]	73.8 ± 0.6	(Ag) ₂ ,Ab and/or Ag,Ab	76.3
		61.5 [Ag,Ab]			
	3.600 ± 0.003	61.5 [Ag,Ab]	43.5 ± 1.0	Ag,Ab and/or Ag	23.7
TcdA-A2 + A20-A26	3.479 ± 0	61.1 [Ag,Ab]	55.1 ± 0.2	Ag,Ab	91.2
	–	–	–	–	4.7
	–	–	–	–	3.3
TcdA-A2 + A26-A20	3.088 ± 0.001	122.2 [(Ag) ₂ ,(Ab) ₂]	108.4 ± 0.8	(Ag) ₂ ,(Ab) ₂	54.6
	3.269 ± 0	93.2 [(Ag) ₂ ,Ab]	102.6 ± 2.0	(Ag) ₂ ,Ab and/or Ag, (Ab) ₂	42.7
		90.1 [Ag,(Ab) ₂]			
–	–	–	–	2.1	
TcdA-A2 + A20-A26 (G ₄ S)	3.077 ± 0.002	121.4 [(Ag) ₂ ,(Ab) ₂]	103.3 ± 0.6	(Ag) ₂ ,(Ab) ₂	46.9
	3.438 ± 0.002	60.6 [Ag,Ab]	66.8 ± 2.0	Ag,Ab	53.0
TcdA-A2 + A20-A26 (G ₄ S) ₂	3.065 ± 0.003	121.8 [(Ag) ₂ ,(Ab) ₂]	116.6 ± 0.3	(Ag) ₂ ,(Ab) ₂	9.2
	3.436 ± 0.003	60.9 [Ag,Ab]	56.4 ± 0.6	Ag,Ab	90.8

Ag, TcdA-A2; Ab, V_HH monomer or dimer depending on sample; T_r , column retention time; M_r , theoretical molecular mass; M_{obs} , observed molecular mass determined by MALS UV. Values are mean ± SD with from two technical replicates. ^aTotal may not add to 100% in some cases, due to minor peaks not identified in the analysis. Relative proportion is only for the representative data plotted in Figure 4. ^bPeaks with <5% relative proportion were omitted from species assignment.

compared to monomeric A26 and A20 based on IC_{99} . While this dramatic increase in potency is likely driven by avidity, the steric disruption of receptor binding due to the larger footprint of A20-A26 may also be important.

In contrast, and as predicted from the crystal structures, the reverse orientation of this construct with A26 positioned N-terminal to A20 was much less effective (29,000-fold less potent) at neutralizing TcdA cytotoxicity. The bivalent monoparatopic constructs (A20-A20 and A26-A26), and the anti-TcdA mAb (CDA1 or actoxumab), also show much poorer neutralization activity than A20-A26. To further explore the effects of length and flexibility in the GS-based linkers, we also produced A20-A26 constructs separated by spacer lengths of 5-, 10-, and 15-amino acids. All of these designs were almost as potent as the

original version of A20-A26 containing a 12-residue linker, in which the length was suggested by a crude and simplistic model for the linker adopting a fully extended conformation. Combinations of individual V_HHs demonstrated poorer efficacy than the top design, pointing to a need for simultaneous engagement of both binding arms by the same antibody molecule to achieve potent cytotoxicity inhibition improvements, an observation reminiscent of analogous multivalent antibody designs evaluated for ricin (Herrera et al., 2015, 2016).

It is important to note that the IC_{50} and IC_{99} of A20-A26 were essentially the same, 0.16 nM and 0.27 nM, respectively, highlighting the highly cooperative nature of its binding to TcdA. In contrast, for other constructs such as A26, A26-A26, and A26-A20, wide gaps between IC_{50} and IC_{99} values were observed. In particular, an IC_{50} of ~50 nM and an

IC_{99} of $\sim 7,900$ nM, an increase of ~ 160 -fold, was observed for the A26-A20 construct. Based on IC_{99} values, A20-A26 showed a 2,700-fold improvement in potency compared to A26 monomer, and a similar improvement with respect to A26-A26. However, it displayed a much higher potency improvement (29,000-fold) relative to A26-A20 due to the much higher IC_{99} of A26-A20 (7,866 nM [A26-A20] vs 719 nM [A26] vs 1,189 nM [A26-A26]). These results suggest that since the A20 moiety binds TcdA more strongly than the A26 moiety of the A26-A20 construct, the A20 moiety may actually sequester the A26 moiety away from the neutralizing A26 epitope, leading to a much higher IC_{99} for A26-A20 compared to A26 or A26-A26. While this does not explain why A20, A20-A20, and A26-A20 have similar IC_{50} s, it does point to the unexpected structural and functional subtleties that arise as a consequence of antibody multimerization, even in the case of very simple multimerization designs such as the linear, flexible linkers used in this study.

SEC-MALS analyses, when considered alongside the neutralization data, reveal that A20-A26 achieves ultra-high TcdA inhibition through a biparatopic interaction with 1:1 stoichiometry (Mode 1; Figure 4A). SEC-MALS also suggests that A20-A26 constructs with 10 [A20-A26 (G_4S)₂] and 12 [A20-A26] residue linkers likely have sufficient length and flexibility to allow both V_{HH} domains to simultaneously engage with the same molecule of TcdA to form a biparatopic Ab.Ag complex. In comparison, the A20-A26 construct with a shorter five-residue linker [A20-A26 (G_4S)] does not appear to readily bind a single molecule of TcdA with high affinity, presumably because the shorter linker prevents both V_{HH} domains from simultaneously engaging with the same molecule of TcdA. Somewhat surprisingly, this construct is still able to neutralize TcdA with a similar level of potency to A20-A26 and A20-A26 (G_4S)₂. SEC-MALS suggests that this is accomplished by two biparatopic V_{HH} - V_{HH} fusion protein molecules simultaneously engaging with two TcdA molecules in a second, biparatopic (Ab)₂. (Ag)₂ interaction (Mode 2), which is presumably nearly as effective a neutralizing mechanism as the intramolecular biparatopic one (Mode 1). Both Mode 1 and Mode 2 binding arrangements involve avidity in solution, i.e., in the toxin neutralization assay setting. This explains why the overall impact of linker length on TcdA neutralization potency for all of these A20-A26 constructs was largely negligible at the TcdA concentrations used in the Vero cell neutralization assays. However, given that Mode 1 biparatopic complex structures are less disturbed by changes in concentrations than Mode 2 biparatopic complex structures, it is likely that A20-A26 would be a more potent inhibitor than A20-A26 (G_4S) at lower, pathologically relevant, TcdA concentrations. The opposite orientation (A26-A20) and monoparatopic controls (A20-A20, A26-A26) are much less effective at neutralizing TcdA due to a lack of avidity when binding to the toxin, although they did display high apparent binding affinities from bivalent engagement in artificial settings (ELISA, SPR). Based on our previous crystal structures (Ho et al., 2005; Greco et al., 2006; Murase et al., 2014) and the work of others (Pruitt et al., 2010; Chumbler et al., 2016; Chen et al., 2022; Kordus et al., 2022), we hypothesize that the bidentate engagement of A20-A26 with TcdA may lead to ultra-potent toxin inhibition through three possible mechanisms: (i) A20-A26 may block enough of the carbohydrate binding pockets in TcdA to substantially disrupt binding interactions between TcdA and cell-surface carbohydrate receptors; (ii) A20-A26 may inhibit pH-induced TcdA

conformational changes that are required for cellular toxicity (Pruitt et al., 2010; Chumbler et al., 2016; Chen et al., 2022); and (iii) we previously deduced the importance of the extreme C-terminus of TcdA playing a role in toxicity (Murase et al., 2014), based on the A26 V_{HH} monomer binding at this region of the toxin and neutralizing TcdA relatively effectively (Hussack et al., 2011). It is also instructive to consider studies on anti-ricin antibodies, where Herrera et al. (2016) showed that separate V_{HH} domains in bispecific anti-ricin antibody fusions neutralized the toxin through a mechanism that involved a single antibody fusion binding more than a single toxin molecule.

In conclusion, we have validated a structure-guided approach for designing a highly-potent *C. difficile* TcdA inhibitor. In the process we show the importance of V_{HH} orientation and geometry in biparatopic constructs, the impact of linker length, and the mode of V_{HH} :toxin interactions on achieving ultra-high neutralization potencies.

Data availability statement

The original contributions presented in the study are included in the article/supplementary material, further inquiries can be directed to the corresponding authors.

Author contributions

GH and JT conceived experiments, analyzed data, and wrote the manuscript. MR performed protein expression and purification, SDS-PAGE, SEC, ELISA, and neutralization assays, analyzed data, and edited the manuscript. HF performed SPR experiments and analyzed data. TM and LE performed SEC experiments and contributed reagents. JS designed and analyzed SEC-MALS experiments and edited the manuscript. KN conceived experiments, analyzed data, and edited the manuscript. All authors contributed to the article and approved the submitted version.

Funding

This work was supported by internal funding from the National Research Council Canada, Project Grant TP4 from the Canadian Glycomics Network to KN and JT, and NSERC Discovery Grant 05287 to KN.

Acknowledgments

We thank Yves Durocher and Denis L'Abbé (NRC) for expression and purification of CDA1 and MDX1388 mAbs, and Petra Pohankova (NRC) for assistance with SEC-MALS experiments.

Conflict of interest

The authors declare that the research was conducted in the absence of any commercial or financial relationships that could be construed as a potential conflict of interest.

Publisher's note

All claims expressed in this article are solely those of the authors and do not necessarily represent those of their affiliated

organizations, or those of the publisher, the editors and the reviewers. Any product that may be evaluated in this article, or claim that may be made by its manufacturer, is not guaranteed or endorsed by the publisher.

References

- Chen, B., Basak, S., Chen, P., Zhang, C., Perry, K., Tian, S., et al. (2022). Structure and conformational dynamics of *Clostridioides difficile* toxin A. *Life Sci. Alliance* 5:e202201383. doi: 10.26508/lsa.202201383
- Chen, P., Lam, K. H., Liu, Z., Mindlin, F. A., Chen, B., Gutierrez, C. B., et al. (2019). Structure of the full-length *Clostridium difficile* toxin B. *Nat. Struct. Mol. Biol.* 26, 712–719. doi: 10.1038/s41594-019-0268-0
- Chumblor, N. M., Rutherford, S. A., Zhang, Z., Farrow, M. A., Lisher, J. P., Farquhar, E., et al. (2016). Crystal structure of *Clostridium difficile* toxin A. *Nat. Microbiol.* 1:15002. doi: 10.1038/nmicrobiol.2015.2
- Durocher, Y., Perret, S., and Kamen, A. (2002). High-level and high-throughput recombinant protein production by transient transfection of suspension-growing human 293-EBNA1 cells. *Nucleic Acids Res.* 30, 9e–99e. doi: 10.1093/nar/30.2.e9
- Fu, Y., Luo, Y., and Grinspan, A. M. (2021). Epidemiology of community-acquired and recurrent *Clostridioides difficile* infection. *Ther. Adv. Gastroenterol.* 14:175628482110162. doi: 10.1177/17562848211016248
- Greco, A., Ho, J. G., Lin, S. J., Palcic, M. M., Rupnik, M., and Ng, K. K. (2006). Carbohydrate recognition by *Clostridium difficile* toxin A. *Nat. Struct. Mol. Biol.* 13, 460–461. doi: 10.1038/nsmb1084
- Henderson, M., Bragg, A., Fahim, G., Shah, M., and Hermes-DeSantis, E. R. (2017). A review of the safety and efficacy of vaccines as prophylaxis for *Clostridium difficile* infections. *Vaccines (Basel)* 5:25. doi: 10.3390/vaccines5030025
- Herrera, C., Klokk, T. I., Cole, R., Sandvig, K., and Mantis, N. J. (2016). A bispecific antibody promotes aggregation of ricin toxin on cell surfaces and alters dynamics of toxin internalization and trafficking. *PLoS One* 11:e0156893. doi: 10.1371/journal.pone.0156893
- Herrera, C., Tremblay, J. M., Shoemaker, C. B., and Mantis, N. J. (2015). Mechanisms of ricin toxin neutralization revealed through engineered homodimeric and heterodimeric camelid antibodies. *J. Biol. Chem.* 290, 27880–27889. doi: 10.1074/jbc.M115.658070
- Hmila, I., Abdallah, R. B., Saerens, D., Benlasfar, Z., Conrath, K., Ayeb, M. E., et al. (2008). VHH, bivalent domains and chimeric heavy chain-only antibodies with high neutralizing efficacy for scorpion toxin AaH1. *Mol. Immunol.* 45, 3847–3856. doi: 10.1016/j.molimm.2008.04.011
- Hmila, I., Saerens, D., Ben Abderrazek, R., Vincke, C., Abidi, N., Benlasfar, Z., et al. (2010). A bispecific nanobody to provide full protection against lethal scorpion envenoming. *FASEB J.* 24, 3479–3489. doi: 10.1096/fj.09-148213
- Ho, J. G., Greco, A., Rupnik, M., and Ng, K. K. (2005). Crystal structure of receptor-binding C-terminal repeats from *Clostridium difficile* toxin A. *Proc. Natl. Acad. Sci. U. S. A.* 102, 18373–18378. doi: 10.1073/pnas.0506391102
- Huang, N. J., Pishesha, N., Mukherjee, J., Zhang, S., Deshycka, R., Sudaryo, V., et al. (2017). Genetically engineered red cells expressing single domain camelid antibodies confer long-term protection against botulinum neurotoxin. *Nat. Commun.* 8:423. doi: 10.1038/s41467-017-00448-0
- Hussack, G., Arbabi-Ghahroudi, M., van Faassen, H., Songer, J. G., Ng, K. K., MacKenzie, R., et al. (2011). Neutralization of *Clostridium difficile* toxin A with single-domain antibodies targeting the cell receptor binding domain. *J. Biol. Chem.* 286, 8961–8976. doi: 10.1074/jbc.M110.198754
- Hussack, G., Ryan, S., van Faassen, H., Rossotti, M., MacKenzie, C. R., and Tanha, J. (2018). Neutralization of *Clostridium difficile* toxin B with V_HH-Fc fusions targeting the delivery and CROPs domains. *PLoS One* 13:e0208978. doi: 10.1371/journal.pone.0208978
- Hussack, G., and Tanha, J. (2016). An update on antibody-based immunotherapies for *Clostridium difficile* infection. *Clin. Exp. Gastroenterol.* 9, 209–224. doi: 10.2147/CEG.S84017
- Katsamba, P. S., Navratilova, I., Calderon-Cacia, M., Fan, L., Thornton, K., Zhu, M., et al. (2006). Kinetic analysis of a high-affinity antibody/antigen interaction performed by multiple Biacore users. *Anal. Biochem.* 352, 208–221. doi: 10.1016/j.ab.2006.01.034
- Kim, D. Y., Kandalaf, H., Ding, W., Ryan, S., van Faassen, H., Hiramata, T., et al. (2012). Disulfide linkage engineering for improving biophysical properties of human V_H domains. *Protein Eng. Des. Sel.* 25, 581–590. doi: 10.1093/protein/gzs055
- Kordus, S. L., Thomas, A. K., and Lacy, D. B. (2022). *Clostridioides difficile* toxins: mechanisms of action and antitoxin therapeutics. *Nat. Rev. Microbiol.* 20, 285–298. doi: 10.1038/s41579-021-00660-2
- Kyne, L., Warny, M., Qamar, A., and Kelly, C. P. (2000). Asymptomatic carriage of *Clostridium difficile* and serum levels of IgG antibody against toxin A. *N. Engl. J. Med.* 342, 390–397. doi: 10.1056/NEJM200002103420604
- Kyne, L., Warny, M., Qamar, A., and Kelly, C. P. (2001). Association between antibody response to toxin A and protection against recurrent *Clostridium difficile* diarrhoea. *Lancet* 357, 189–193. doi: 10.1016/S0140-6736(00)03592-3
- Lam, K. H., Tremblay, J. M., Vazquez-Cintron, E., Perry, K., Ondeck, C., Webb, R. P., et al. (2020). Structural insights into rational design of single-domain antibody-based antitoxins against botulinum neurotoxins. *Cell Rep.* 30, 2526–2539.e6. doi: 10.1016/j.celrep.2020.01.107
- Leav, B. A., Blair, B., Leney, M., Knauber, M., Reilly, C., Lowy, I., et al. (2010). Serum anti-toxin B antibody correlates with protection from recurrent *Clostridium difficile* infection (CDI). *Vaccine* 28, 965–969. doi: 10.1016/j.vaccine.2009.10.144
- Mejías, M. P., Hiriart, Y., Lauché, C., Fernández-Brando, R. J., Pardo, R., Bruballa, A., et al. (2016). Development of camelid single chain antibodies against Shiga toxin type 2 (Stx2) with therapeutic potential against hemolytic uremic syndrome (HUS). *Sci. Rep.* 6:24913. doi: 10.1038/srep24913
- Moayeri, M., Leysath, C. E., Tremblay, J. M., Vrentas, C., Crown, D., Leppla, S. H., et al. (2015). A heterodimer of a VHH (variable domains of camelid heavy chain-only) antibody that inhibits anthrax toxin cell binding linked to a VHH antibody that blocks oligomer formation is highly protective in an anthrax spore challenge model. *J. Biol. Chem.* 290, 6584–6595. doi: 10.1074/jbc.M114.627943
- Mukherjee, J., Tremblay, J. M., Leysath, C. E., Ofori, K., Baldwin, K., Feng, X., et al. (2012). A novel strategy for development of recombinant antitoxin therapeutics tested in a mouse botulism model. *PLoS One* 7:e29941. doi: 10.1371/journal.pone.0029941
- Murase, T., Eugenio, L., Schorr, M., Hussack, G., Tanha, J., Kitova, E. N., et al. (2014). Structural basis for antibody recognition in the receptor-binding domains of toxins A and B from *Clostridium difficile*. *J. Biol. Chem.* 289, 2331–2343. doi: 10.1074/jbc.M113.505917
- Pruitt, R. N., Chambers, M. G., Ng, K. K., Ohi, M. D., and Lacy, D. B. (2010). Structural organization of the functional domains of *Clostridium difficile* toxins A and B. *Proc. Natl. Acad. Sci. U. S. A.* 107, 13467–13472. doi: 10.1073/pnas.1002199107
- Pruitt, R. N., and Lacy, D. B. (2012). Toward a structural understanding of *Clostridium difficile* toxins A and B. *Front. Cell. Infect. Microbiol.* 2:28. doi: 10.3389/fcimb.2012.00028
- Rossotti, M. A., González-Tejera, A., Guarnaschelli, J., Yim, L., Camacho, X., Fernández, M., et al. (2015). Increasing the potency of neutralizing single-domain antibodies by functionalization with a CD11b/CD18 binding domain. *MABS* 7, 820–828. doi: 10.1080/19420862.2015.1068491
- Schmidt, D. J., Beamer, G., Tremblay, J. M., Steele, J. A., Kim, H. B., Wang, Y., et al. (2016). A tetraspecific VHH-based neutralizing antibody modifies disease outcome in three animal models of *Clostridium difficile* infection. *Clin. Vaccine Immunol.* 23, 774–784. doi: 10.1128/CVI.00730-15
- Shogbesan, O., Poudel, D. R., Victor, S., Jehangir, A., Fadahunsi, O., Shogbesan, G., et al. (2018). A systematic review of the efficacy and safety of fecal microbiota transplant for *Clostridium difficile* infection in immunocompromised patients. *Can. J. Gastroenterol. Hepatol.* 2018, 1–10. doi: 10.1155/2018/1394379
- Tremblay, J. M., Mukherjee, J., Leysath, C. E., Debatis, M., Ofori, K., Baldwin, K., et al. (2013). A single VHH-based toxin-neutralizing agent and an effector antibody protect mice against challenge with Shiga toxins 1 and 2. *Infect. Immun.* 81, 4592–4603. doi: 10.1128/IAI.01033-13
- Tremblay, J. M., Vazquez-Cintron, E., Lam, K. H., Mukherjee, J., Bedence, D., Ondeck, C. A., et al. (2020). Camelid VHH antibodies that neutralize botulinum neurotoxin serotype E intoxication or protease function. *Toxins (Basel)* 12:611. doi: 10.3390/toxins12100611
- Vance, D. J., Tremblay, J. M., Mantis, N. J., and Shoemaker, C. B. (2013). Stepwise engineering of heterodimeric single domain camelid V_HH antibodies that passively protect mice from ricin toxin. *J. Biol. Chem.* 288, 36538–36547. doi: 10.1074/jbc.M113.519207
- Vasilescu, I. M., Chifiriuc, M. C., Pircalabioru, G. G., Filip, R., Bolocan, A., Lazăr, V., et al. (2021). Gut dysbiosis and *Clostridioides difficile* infection in neonates and adults. *Front. Microbiol.* 12:651081. doi: 10.3389/fmicb.2021.651081
- Vrentas, C. E., Moayeri, M., Keefer, A. B., Greaney, A. J., Tremblay, J., O'Mard, D., et al. (2016). A diverse set of single-domain antibodies (VHHs) against the anthrax toxin lethal and edema factors provides a basis for construction of a bispecific agent that protects against anthrax infection. *J. Biol. Chem.* 291, 21596–21606. doi: 10.1074/jbc.M116.749184
- Wade, J., Rimbault, C., Ali, H., Ledsgaard, L., Rivera-de-Torre, E., Abou Hachem, M., et al. (2022). Generation of multivalent nanobody-based proteins with improved neutralization of long α -neurotoxins from elapid snakes. *Bioconjug. Chem.* 33, 1494–1504. doi: 10.1021/acs.bioconjchem.2c00220
- Wilcox, M. H., Gerding, D. N., Poxton, I. R., Kelly, C., Nathan, R., Birch, T., et al. (2017). Bezlotoxumab for prevention of recurrent *Clostridium difficile* infection. *N. Engl. J. Med.* 376, 305–317. doi: 10.1056/NEJMoa1602615
- Yang, Z., Schmidt, D., Liu, W., Li, S., Shi, L., Sheng, J., et al. (2014). A novel multivalent, single-domain antibody targeting TcdA and TcdB prevents fulminant *Clostridium difficile* infection in mice. *J. Infect. Dis.* 210, 964–972. doi: 10.1093/infdis/jiu196